Shack–Hartmann sensor based on a cylindrical microlens array

M. Ares, S. Royo, and J. Caum

Center for Sensor, Instrumentation and System Development, Technical University of Catalonia (CD6-UPC), Rambla Sant Nebridi 10, 08222 Terrassa, Spain

Received November 3, 2006; revised December 21, 2006; accepted December 24, 2006; posted January 8, 2007 (Doc. ID 76759); published March 5, 2007

We present a Shack–Hartmann wavefront sensor (SHWS) based on a cylindrical microlens array as a device for measuring highly aberrated wavefronts. Instead of the typical spot pattern created by a conventional SHWS, two orthogonal line patterns are detected on a CCD and are superimposed. A processing algorithm uses the continuity of the focal line to extend the dynamic range of measurement by localizing the line, even if it leaves the CCD area confined by the corresponding microcylinder. The measurement of a wavefront from a progressive addition lens with an 80 λ peak-to-valley value reveals the capabilities of the sensor. © 2007 Optical Society of America

OCIS codes: 120.2650, 120.3930, 120.3940, 120.5050.

The Shack–Hartmann wavefront sensor (SHWS) is a well-known setup for measuring wavefront shapes.[1,2] In a single shot, the wavefront is spatially sampled using a microlens array that creates a spot pattern on a photodetector (typically a CCD camera) placed at the focal distance of the microlenses. The displacement of the spots created by the wavefront to be measured from the spots of a reference wavefront (usually a plane beam) allows for the measurement of the average wavefront slopes across each microlens aperture. The original wavefront shape is usually obtained by fitting them to a polynomial basis.[3,4]

Although typical resolutions of the SHWS are not as high as those obtained in interferometry, the SHWS has a much larger dynamic range and a larger tolerance to non-vibration-isolated environments. The trade-off between resolution and dynamic range must be managed in the design of the sensor by choosing the *f* number of the lenslet that matches the requirements of the specific application.[5] To measure the wavefront correctly, each of the detected spots must be assigned unequivocally to the microlens that refracted it. In the classical SHWS, samples are required to lie in the photodetector area corresponding to a given microlens, so the dynamic range becomes quite limited. A great deal of effort has been devoted to developing schemes for extending the dynamic range of the sensor once the *f* number is fixed.[6,7]

To deal with highly aberrated wavefronts with abrupt shape changes, we propose a SHWS based on a cylindrical microlens array. Thus, we replace the conventional array of spherical microlenses with an array of microcylinders that focuses the wavefront to be measured onto the CCD in the form of focal lines, instead of focal spots. This means that spots in a given focal line are now continuously connected, allowing us to perform a correct assignment of all the data, even in cases when the wavefront has locally important slope changes. The two-dimensional information on slope that is present on a spot pattern is obtained by superimposing the two line patterns with the microcylinders oriented in orthogonal directions.

The expansion of dynamic range using a cylindrical microlens array is illustrated in Fig. 1. A typical spot and vertical line patterns from a complex-shaped wavefront passing through a conventional SHWS and through the sensor that we propose have been drawn as an example. The part of the wavefront that passes through the central column of the array of spherical microlenses (numbered as 1) or through the central microcylinder (1) is properly localized in both cases. However, regarding areas 3 and 5, it may be seen how in the conventional SHWS the spots tagged with capital letters leave their original subapertures in area 3 and merge with those belonging to area 5. This implies an uncertainty in the assignment of spots a5 and A5, b5 and B?, and g5 and G5, and, consequently, a loss of these data for wavefront reconstruction. The use of an array of cylindrical microlenses solves this problem as all the wavefront samples refracted by each microcylinder are connected in the same focal line and could be easily tracked. Thus, samples within line numbers 5 and 3 are assigned to microcylinders 5 and 3, respectively.

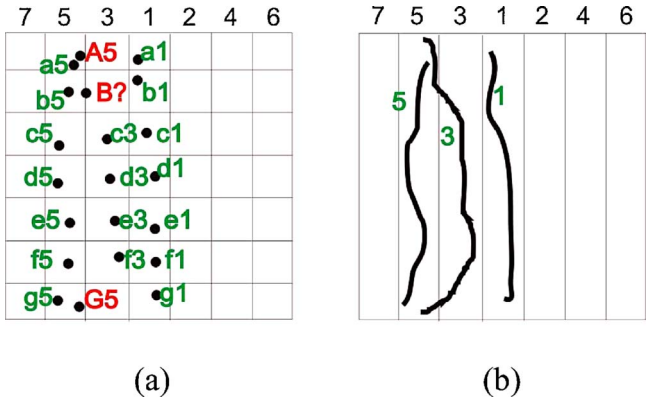

Fig. 1. (Color online) Example to illustrate the detected patterns of a complex wavefront with (a) a conventional SHWS with spherical microlenses that has an uncertainty on the localization of spots a5 and A5, b5 and B?, and g5 and G5; and (b) our sensor based on an array of microcylinders from which all the data are unequivocally localized.

0146-9592/07/070769-3/$15.00

The experimental setup developed to test the described measurement principle is depicted in Fig. 2. A 635 nm laser diode coupled with a monomode optical fiber acts as a point source that is collimated using a diffraction-limited achromat. The collimated beam crosses the optical object of interest, and the transmitted wavefront is conjugated with a cylindrical microlens array through an afocal 4:1 beam-reducer system. Microcylinders of $f=10.9$ mm focal length and $d=500\ \mu$m width sample the wavefront, creating a focal line pattern recorded by a monochrome CCD detector of pixel dimensions $p_x=p_y=4.65\ \mu$m. The array is placed onto a high-precision rotary stage, which allows the vertical and horizontal line patterns to be recorded. Once the two orthogonal line patterns are captured, a processing algorithm is applied, which localizes the lines, even if they leave their corresponding microcylinder areas. First, in each line pattern, a segmentation procedure separates the connected active pixels from the background. Next, each of the resulting lines is tagged with ascending X and Y values starting from the central cylindrical microlens. Once each of the lines is tagged, both line patterns are superimposed and the areas with the active pixels of the intersection are obtained. These areas are equivalent to the spots of a conventional SHWS. The centroids $(\rho_x^{(X,Y)}, \rho_y^{(X,Y)})$ of these active areas are calculated using a classical center-of-mass computation. The wavefront slopes in the x and y directions (using the displacement of the aberrated centroids from the corresponding ones of the reference wavefront) are then calculated following the usual SHWS geometrical approximation:

$$u^{(X,Y)} = \frac{\partial W}{\partial x} = \frac{M(\rho_{x,\mathrm{ABERR}}^{(X,Y)} - \rho_{x,\mathrm{REF}}^{(X,Y)})p\_x}{f},$$

$$v^{(X,Y)} = \frac{\partial W}{\partial y} = \frac{M(\rho_{y,\mathrm{ABERR}}^{(X,Y)} - \rho_{y,\mathrm{REF}}^{(X,Y)})p\_y}{f}, \qquad (1)$$

where $M=\frac{1}{4}$ is the magnification of the afocal system. From these data, the wavefront is easily reconstructed in terms of the circular Zernike polynomial decomposition.[8]

An important issue to be considered is the calibration of the proposed sensor. In a first approximation, there are two main sensor parameters for which a difference between the real and nominal values may affect the accuracy of the measurement: the CCD pixel size and the spacing between the rear principal plane of the lenslet array and the CCD chip (focal length of the microlenses).[9] We calibrated the sensor using the spherical wavefront created by the fiber-optic point light source of our system. The fiber tip was placed 535 mm in front of the object plane of the 4:1 beam reducer. By simply removing the collimating lens, the divergent spherical wavefront with a well-known 535 mm radius of curvature (ROC) must be sensed. The plane wave created when the large achromat is working as a collimator is used as the reference beam. This calibration has two main advantages: (a) the same collimated wavefront used as the reference in the calibration will be used when measuring any phase object, and (b) a high-quality spherical wavefront has been used for calibration without any mechanical changes to the experimental setup, avoiding the introduction of potential additional errors.

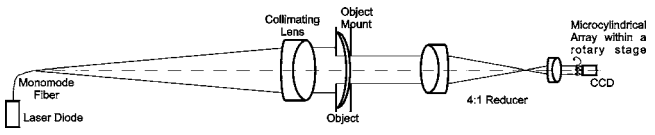

Fig. 2. Scheme of the setup to test an object by transmission with the cylindrical microlens array sensor.

By means of a linear fit of the displacement of the reference and the aberrated centroids for the x (y) positions, the curvature, C, of the measured spherical wavefront multiplied by the $(p\_x/f)^{-1}((p\_y/f)^{-1})$ factor was obtained. Taking into consideration that the reference curvature of the spherical wavefront is $C=(\mathrm{ROC}\cdot M^2)^{-1}=(535\cdot 1/4^2)^{-1}\ \mathrm{mm}^{-1}$ because of the 4:1 afocal reducer, we got p_x/f and p_y/f calibrated values of 4.685×10^{-4} and 4.687×10^{-4}. The spherical wavefront measurement was also used to compute the sensitivity (or vertical resolution) of the sensor, defined as the smallest amount of wavefront aberration that the sensor can reliably measure. Ten successive measurements were taken. From these, the rms difference between the measured u and v slopes and the average slopes was calculated. A rms value of 0.017 mrad was obtained. From that slope sensitivity, calculating the sensitivity of the sensor in terms of the wavefront is straightforward using the relation proposed by Neal *et al.*[10]:

$$\text{rms wavefront error} = (\text{rms slope error})d\sqrt{N}, \quad (2)$$

where N is the number of samples and d is the width of the microlenses. This results in a sensitivity of $\lambda/25$ at the wavelength used ($\lambda=635$ nm).

To show the capabilities of the system, we measured a commercial progressive addition lens (PAL) that had nominal null far vision power and +2D power addition. A 20 mm diameter area was inspected, covering the power progression corridor and part of the lateral blurred zones where considerable astigmatism is present. The intersection between the two orthogonal line patterns recorded by the CCD is shown in Fig. 3(a). The deflection of the focal lines visually shows the power progression of the PAL from the plane far vision zone to the highest-power near-vision zone. As expected, in the regions where the wavefront is more aberrated, the width of the focal line increases from the diffraction-limited size and is also displaced outside the corresponding microcylinder area on the CCD array. From the 74 u and v pairs measured, we performed the wavefront reconstruction in terms of the Zernike basis. Figure 3(b) shows how the wavefront is almost flat in the far vision area and increases its curvature along the corridor following the increase in lens power. The distribution of astigmatic aberrations in the lateral areas of the vertical corridor is also clearly shown. The measured

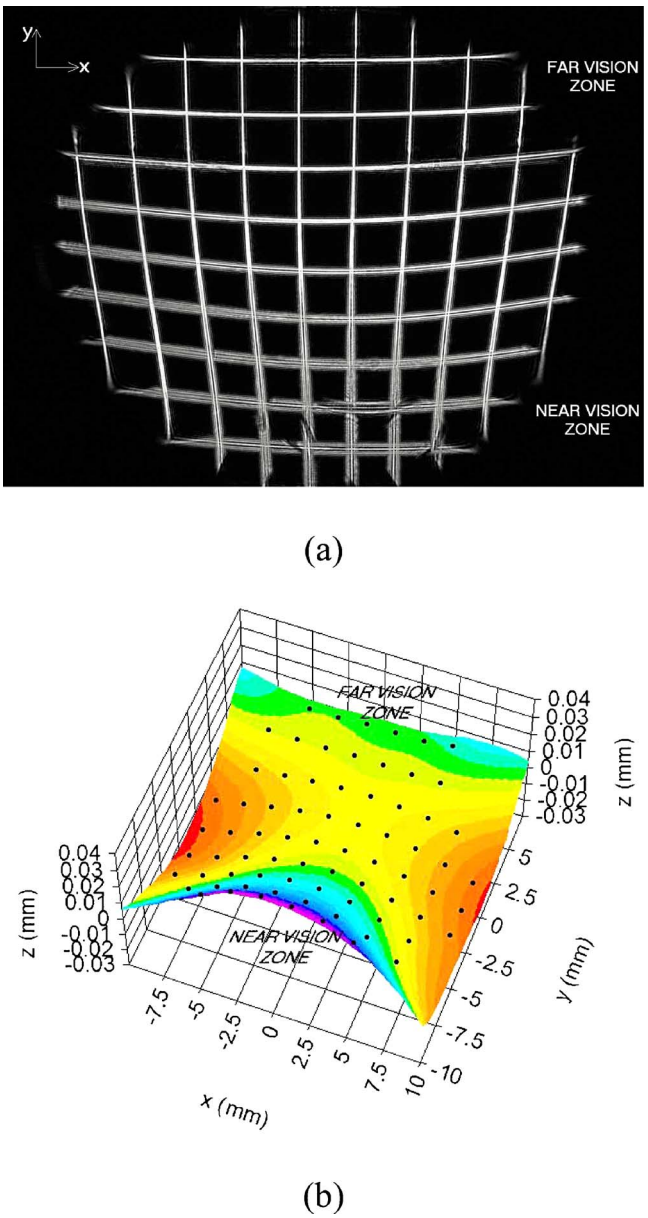

Fig. 3. (Color online) PAL measured with the sensor: (a) intersection of the line patterns in the x and y directions recorded by the CCD, (b) reconstruction of the wavefront transmitted by the PAL.

peak-to-valley (PV) of more than 80λ reveals the huge dynamic range of the sensor.

Summarizing, we have developed a SHWS sensor based on a cylindrical microlens array. The use of cylindrical microlenses combined with the image processing algorithm presented extends the dynamic range of the conventional SHWS sensor, allowing for the measurement of highly aberrated wavefronts. To improve measurement accuracy, the sensor was calibrated using a simple method. A sensor sensitivity of $\lambda/25$ at $\lambda = 635$ nm was also obtained. Finally, a wavefront transmitted by a commercial PAL with more than 80λ PV height was tested with the sensor to demonstrate its complex-shaped wavefront measurement performance.

The authors thank the Spanish Ministry of Education and Science for the AP2003-3140 grant received, and for the project DPI2005-00828, which has partially funded this research. M. Ares's e-mail address is miguel.ares@oo.upc.edu.

References

1. G. Y. Yoon, T. Jitsuno, M. Nakatsuka, and S. Nakai, Appl. Opt. **35**, 188 (1996).
2. T. M. Jeong, M. Menon, and G. Yoon, Appl. Opt. **44**, 4523 (2005).
3. J. Primot, G. Rousset, and J. C. Fontanella, J. Opt. Soc. Am. A **7**, 1598 (1990).
4. L. Seifert, H. J. Tiziani, and W. Osten, Opt. Commun. **245**, 255 (2005).
5. R. R. Rammage, D. R. Neal, and R. J. Copland, Proc. SPIE **4779**, 161 (2002).
6. N. Lindlein and J. Pfund, Opt. Eng. **41**, 529 (2002).
7. J. Lee, R. V. Shack, and M. R. Descour, Appl. Opt. **44**, 4838 (2005).
8. D. Malacara and S. L. DeVore, *Optical Shop Testing* (Wiley, 1992), p. 461.
9. A. Chernyshov, U. Sterr, F. Riehle, J. Helmcke, and J. Pfund, Appl. Opt. **44**, 6419 (2005).
10. D. R. Neal, D. J. Armstrong, and W. T. Turner, Proc. SPIE **2993**, 211 (1997).